Chemical Science

ROYAL SOCIETY OF CHEMISTRY

EDGE ARTICLE

View Article Online
View Journal | View Issue

Cite this: *Chem. Sci.*, 2023, **14**, 9063

All publication charges for this article have been paid for by the Royal Society of Chemistry

Received 29th March 2023
Accepted 18th June 2023

DOI: 10.1039/d3sc01629c

rsc.li/chemical-science

Nanocapsules of unprecedented internal volume seamed by calcium ions†

Kanishka Sikligar,[a] Steven P. Kelley,[a] Durgesh V. Wagle,[b] Piyuni Ishtaweera,[a] Gary A. Baker *[a] and Jerry L. Atwood *[a]

The inception of an unprecedented class of voluminous Platonic solids displaying hierarchical geometry based on pyrogallol[4]arene moieties seamed by divalent calcium ion is described. Single-crystal X-ray structural determination has established the highly conserved geometry of two original Ca^{2+}-seamed nanocapsules to be essentially cubic in shape with *C*-ethylpyrogallol[4]arene units located along the twelve edges of the cube which are then bridged by metallic polyatomic cations ($[Ca_4Cl]^{7+}$ or $[Ca(HCO_2)Na_4]^{5+}$) at the six cube faces. The accessible volume of the nanocapsules is *ca.* 3500 Å^3 and 2500 Å^3 and is completely isolated from the exterior of the capsules. These remarkable nanocapsule discoveries cast a spotlight on a marginalized area of synthetic materials chemistry and encourage future exploration of diversiform supramolecular assemblies, networks, and capsules built on calcium, with clear benefits deriving from the intrinsic biocompatibility of calcium. Finally, a proof-of-concept is demonstrated for fluorescent reporter encapsulation and sustained release from the calcium-seamed nanocapsules, suggesting their potential as delivery vehicles for drugs, nutrients, preservatives, or antioxidants.

The development of molecular capsule research began in 1995 with reports by Rebek *et al.* of "tennis ball" assemblies.[1–3] These hydrogen-bonded, self-assembled dimers enclose a volume sufficient to host a methanol molecule ($V_{enclosed} \approx 100$ Å^3). In 1997, MacGillivray and Atwood synthesized and characterized the hexameric [*C*-methylresorcin[4]arene]$_6(H_2O)_8$, a molecular capsule held together by 60 hydrogen bonds and having a $V_{enclosed}$ of ~1400 Å^3.[4] This nanocapsule possessed an overall geometry of the Archimedean solid referred to as a snub cube.[5] Subsequently, it was discovered that *C*-alkylpyrogallol[4]arenes in a range of nonaqueous solvents afforded hexameric capsules held together by 72 hydrogen bonds.[6–8] In 2005, McKinlay *et al.* found that 24 Cu^{2+} ions stripped 48 H^+ ions from the [*C*-propan-3-olpyrogallol[4]arene]$_6$ structure to yield Cu_{24}[*C*-propan-3-olpyrogallol[4]arene]$_6$.[9] Consequently, a range of M_{24}[*C*-alkylpyrogallol[4]arene]$_6$ (hexameric) and M_8[*C*-alkylpyrogallol[4]arene]$_2$ (dimeric) nanocapsules were demonstrated, both in the solid state and in solution, for M = Zn,[10,11] Cu,[12,13] Ni,[13,14] Co,[15,16] Ga,[17,18] In,[19] Fe,[20] Mn,[21,22] V,[23] and U.[24] Furthermore, very recently *C*-butylpyrogallol[4]arene formed an anion-based self-assembly leading to the formation of hexameric nonocapsules that are ion-paired with cations.[25] Although the 24 years of continuous research since the discovery of the hexameric capsule have produced numerous variants of the known hexameric and dimeric structures, almost no examples exist for alternate geometries beyond these two. Solution studies have pointed to the existence of larger geometries, but these have never been isolated.[26] Even nanocapsules built on less usual metals (*e.g.*, alkali or alkaline Earth metals, mixed-valence) or mixed macrocycles, for example Ga_{12}[*C*-alkylpyrogallol[4]arene]$_6$,[17] $(Fe^{2+})_{16}(Fe^{3+})_{16}$[*C*-alkylpyrogallol[4]arene]$_6$,[20] $(Mn^{3+})_4(Mn^{2+})_{21}$[*C*-alkylpyrogallol[4]arene]$_6$,[22] Zn_{18}[(*C*-alkylpyrogallol[3](resorcinarene[1]))]$_6$,[27] and Zn_7[(*C*-alkylpyrogallol[3](resorcinarene[1]))]$_2$,[28] generally represent iterations of earlier-established geometries.

Recently, solvothermal methods have emerged as synthetic tools to prepare varied nanocages,[29,30] including nanocapsules incorporating *C*-alkylpyrogallol[4]arenes.[31–41] Initially, the solvothermal method was employed in the synthesis of discrete nanocapsules with metal ions like magnesium[39,40] and as a tool to alter the geometries of the existing nanocapsules.[27,28] Followingly, the solvothermal method was used to functionalize nanocapsules.[34,42] For instance, the magnesium nanocapsule was functionalized externally (altering the ligand to *C*-propan-3-olpyrogallol[4]arene; PgC_3OH from *C*-propylpyrogallol[4]arene; PgC_3) and internally (coordinating six proline molecules endohedrally).[42] Very recently, solvothermal methods were employed in synthesizing hierarchical self-assemblies from nanocapsules of Dy,[41] Gd,[41] and Pr,[37] advocating the use of solvothermal methods in obtaining diverse[43] and controlled self-assemblies.

[a]*Department of Chemistry, University of Missouri – Columbia, 601 S College Avenue, Columbia, MO – 65211, USA. E-mail: AtwoodJ@missouri.edu; bakergar@missouri.edu*
[b]*Department of Chemistry and Physics, Florida Gulf Coast University, 10501 FGCU Blvd. S., Fort Myers, FL – 33965, USA*

† Electronic supplementary information (ESI) available. CCDC 1955663 and 2071418. For ESI and crystallographic data in CIF or other electronic format see DOI: https://doi.org/10.1039/d3sc01629c

Calcium-based metal–organic frameworks are known[44] however, zero-dimensional calcium-seamed nanocapsules have never been isolated. Such Ca^{2+}-seamed nanocapsules may prove interesting as benign catalytic centers and find biomedical application, given the high natural abundance (3.4% of Earth's core) and biocompatibility of calcium. Calcium ion was recently shown by the Dauenhauer group to accelerate glycosidic ether scission in cellulose,[45] with Ca^{2+} acting primarily to stabilize charged transition states and secondarily in the disruption of native cellulose hydrogen bonding. In another example, Rösch *et al.* reported that β-diketiminate-ligated low-valent Ca^{+} can mediate dinitrogen reduction, assisted by potassium as the terminal reductant.[46] These developments have inspired efforts in our group to expand the chemistry of pyrogallol[4]arene-based nanocapsules to include calcium as the bridging species. Remarkably, a solvothermal treatment of $CaCl_2$ with *C*-ethylpyrogallol[4]arene (PgC_2, Fig. 1) afforded completely unexpected dodecamers comprising giant cube-shaped nanocapsules compositionally described by $[(Ca_4Cl)_6][(C\text{-ethyl-pyrogallol[4]arene})_{12}]$.

The ligand *C*-ethylpyrogallol[4]arene (PgC_2) **1** was prepared by condensation between pyrogallol and propionaldehyde.[40] **1** is a cup-shaped molecule displaying twelve hydroxyl groups positioned at the rim of the cup (Fig. 1). Firstly, a series of experiments were carried out assembling **1** and anhydrous calcium chloride. The ligand **1** when mixed with anhydrous calcium chloride in a 1 : 1 (v/v) DMF : methanol (MeOH) solution, followed by sonication (60 min), and heating of the reaction flask at 125 °C (24 h) afforded golden plate-like crystals of calcium-seamed nanocapsule **2** $[(Ca_4Cl)_6][(PgC_2)_{12}]$, which were structurally characterized by single crystal X-ray diffraction (SCXRD) using a synchrotron light source. We attempted to isolate more examples of this new family of capsules using other Ca^{2+} salts. Mixing ligand **1** with calcium bromide hydrate in 6 mL DMF, followed by sonication (60 min), and heating of the reaction flask at 125 °C (96 h) afforded golden plate-like crystals of an isostructural capsule, this one seamed by a polyatomic ion composed of Ca^{2+}, Na^{+}, and formate (HCO_2^{-}) (nanocapsule **3** $[Ca_{32}(CaNa_4(HCO_2)_5)_6(OH)_8(DMF)_{24}(OH_2)_{54}(PgC_2)_{12}]$). The source of Na^{+} ions in **3** is unknown; attempts to reproduce it by deliberately adding Na^{+} and HCO_2^{-} have only led to the isolation of known crystalline forms of $Ca(HCO_2)_2$. Subsequent attempts to synthesize a capsule using $CaBr_2$ in the absence of Na^{+} and HCO_2^{-} have repeatedly led to the isolation of a homogeneous crystalline phase with a unit cell of comparable volume to **2** and **3** as determined by SCXRD (tetragonal *P*, $a = b = 38.26(2)$ Å, $c = 39.92(2)$ Å, $\alpha = \beta = \gamma = 90°$; $V = 58\,436(2)$ Å^3). The crystal structure has not yet been solved, as all SCXRD measurements on these crystals have failed to produce a data set of sufficient resolution to be solved by small molecule methods. Regardless, the isolation of **2** and **3** indicate that the unusual cubic geometry is reproducible, with as-yet undiscovered variations likely to exist (Fig. 2).

Crystal structure analysis shows that both capsules have 12 PgC_2 moieties on the edges of the cube which are bridged across the faces of the cube by polyatomic ions containing four metal ions in a cross-shaped arrangement (Fig. 3 and S6, S7†). In **2** these consist of discrete, planar groups of 4 Ca^{2+} ions bridged to a single central Cl^{-} (Fig. S8†); similar arrangements have been reported with bridging Cl^{-}, F^{-}, and O_2^{-} ions.[47–49] In capsule **3**, the PgC_2 ligands coordinate to Na^{+} ions which are bridged to a central Ca^{2+} ion in an analogous shape (Fig. S9†). The cubic faces and PgC_2 moieties in **3** are further cross linked by tetranuclear clusters of Ca^{2+} ions bridged by formate (Fig. S10†). The interiors of the capsules are completely sealed from the exterior environments of the capsule. The accessible internal volumes are estimated at 3500 Å^3 and 2500 Å^3 for **2** and **3**, respectively. The smaller internal volume of **3** is due to the fact that the polyatomic ion occupies part of the internal capsule; otherwise, the two capsules are nearly identical in size. Both capsules pack through assorted noncovalent interactions between edges or corners of the cubes, leaving large regions outside the capsules filled with disordered solvent molecules.

As the crystal structures indicate that the nanocapsule interiors are totally isolated from the exterior, these nanocapsules could potentially be used to make large, discrete, and isolated volumes for host–guest applications. Nanocapsule **2** could be crystallized reproducibly and was used to examine the stability of these capsules. Powder X-ray diffraction (PXRD) on a bulk sample of **2** covered in mother liquor and crystals of **2** allowed to dry in ambient air for 1 h are given in Fig. 4A. The diffraction pattern of the fresh slurry at ambient temperature matches

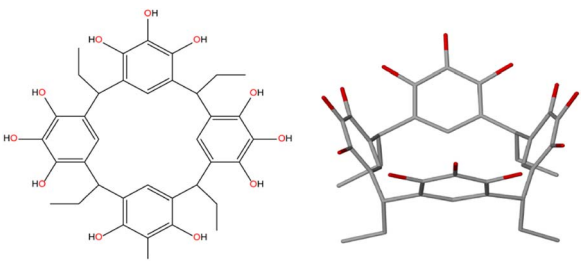

Fig. 1 Structure of the *C*-ethylpyrogallol[4]arene (PgC_2) **1** organic nanocapsule building block. (left) Line drawing and (right) schematic structure showing a cup-shaped geometry. Oxygens are shown in red to highlight the twelve upper rim hydroxyl groups.

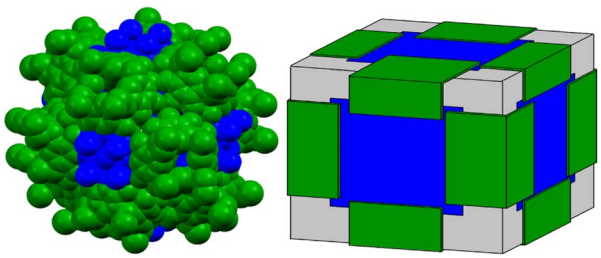

Fig. 2 Summary of Ca^{2+}-seamed nanocapsules. (left) Space-filling and (right) simplified block diagram illustrating the arrangements of the PgC_2 **1** macrocycle building block (green) and bridging polyatomic metal complex (blue; either $([Ca_4Cl]^{7+}$ or $[Ca(HCO_2)Na_4]^{5+}$) within the cube-shaped nanocapsules. The atomic coordinates for the left panel are those of nanocapsule **2** in which each cube face contains the square planar species $[Ca_4Cl]^{7+}$.

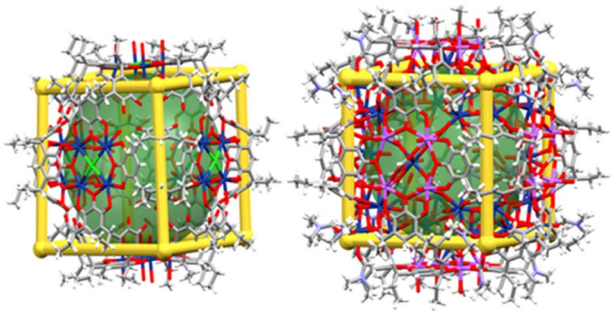

Fig. 3 Packing plots of nanocapsules (left) **2** and (right) **3** formed by reaction of calcium halide and PgC_2. Superimposed gold frames and green spheres are included to accentuate the essentially cubic Platonic geometry and internal cavities, respectively. Elements are color coded as follows: C = gray, H = white, N = pale violet, O = red, Cl = green, Na = orchid, Ca = royal blue.

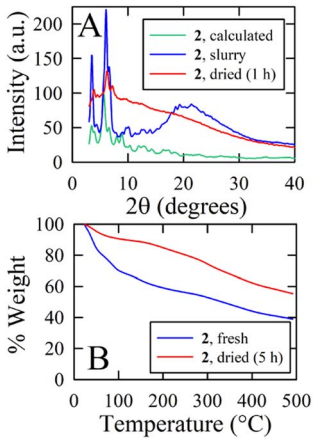

Fig. 4 (A) Powder X-ray diffraction (PXRD) patterns and (B) thermogravimetric analysis (TGA) on samples of **2** that were freshly removed from the mother liquor (blue) or allowed to dry in ambient air (red).

reasonably well to a theoretical pattern predicted from atomic coordinates. The main differences are a number of smaller or missing peaks in the theoretical pattern which likely correspond to atoms removed from the model by the solvent mask. Allowing **2** to dry in air for 1 h results in the loss of all but the lowest angle diffraction peaks; this indicates that much of the crystalline order is lost, most likely due to evaporation of the interstitial solvent, but the structure retains order at its longest length scales, corresponding to the capsules themselves. Thermogravimetric analysis (TGA) shows that both fresh and dried samples of bulk **2** immediately lose mass on heating in a step that stabilizes at *ca.* 100 °C (Fig. 4B). For the fresh sample, this step results in the loss of 30.3% of the sample mass; for comparison, the calculated density of **2** with solvent omitted (0.713 g cm^{-3}) is 34.3% lower than the density of 1.07 g cm^{-3} calculated for $[Mg_{24}(C\text{-propylpyrogallol[4]arene})_6(proline)_6(DMF)_2(Hs_2O)_{30}]$[42] for which the solvent is modeled. The dried sample of **2** loses 9.5% of its mass. The mass loss of the wet sample is triple that of the dried sample, which is similar to the relative sizes of the interstitial voids which are 2.4 times the size of the encapsulated voids (17 425 $Å^3$ *vs.* 7132 $Å^3$ per unit cell, respectively). Together, the PXRD and TGA data indicate that, although the crystals are ultimately unstable to solvent loss even at room temperature, the capsules are apparently stable and are able to prevent loss of the encapsulated solvent until after the loss of the interstitial solvent.

The possibility for hosting functional cargo by entrapping it within the interior environment of calcium-seamed nanocapsules during nanocapsular assembly and crystallization was investigated by synthesizing capsule **2** in the presence of the fluorescent probes Nile red and pyranine (8-hydroxypyrene-1,3,6-trisulfonate). A comparison reveals that the fluorescence spectrum of Nile red (NR) released from **2** upon dissolution in DMSO perfectly matched that of free NR in DMSO (Fig. 5A), both showing a fluorescence maximum at 633 nm. The pyranine was similarly unperturbed by encapsulation within calcium-seamed **2** (data not shown). These experiments indicate that fluorescent cargo can be entrapped within **2** and subsequently released intact.

Dissolution experiments were carried out to obtain the release profiles of NR and pyranine from **2**. Fig. 5B displays the time release behavior of the entrapped fluorescent reporters using 1 : 1 (v/v) dimethylformamide (DMF) : MeOH as the release medium. The calcium-seamed capsules do not dissolve in this medium. After dispersing crystals of NR- or pyranine-containing **2** into 1 : 1 DMF : MeOH, the fluorescent reporter is gradually released by diffusion through the crystalline matrix and into the surrounding medium. The time-resolved fluorescence intensity reveals sustained release of the entrapped fluorescent reporters over the course of an hour. Interestingly, the release profiles differ markedly for NR and pyranine. NR, a fairly small (~300 Da), uncharged, hydrophobic molecule, exhibits significant initial "burst" release, followed by slower additional release over time. The release behavior for pyranine exhibits a much more steady release over the course of an hour. Although both fluorescent reporters are expected to display guest-to-wall binding to

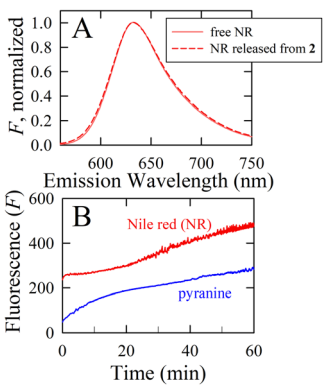

Fig. 5 (A) Normalized steady-state emission spectrum for **2**-encapsulated Nile red (NR) released by crystal dissolution in DMSO compared to the spectrum of the free dye in DMSO. (B) Time-release profiles for Nile red and pyranine encapsulated within **2** during nanocapsular assembly, monitored at 638 nm and 513 nm, respectively. A 1 : 1, v/v DMF : MeOH mixture was used as the extraction solvent at a level of 1.2 mL per mg of **2**.

nanocapsules within **2**, attributable to π stacking and CH···π interactions, the marked difference in release behavior predominantly reflects the highly charged (trianionic) nature but also the larger size (~500 Da) of pyranine. That is, the different time release profiles reflect differences in the guest chemistry, suggesting disparate guest populations and selectivity in binding strength. Although details of the mechanism of entrapment and kinetic release profiles are beyond the scope of this study, these results provide proof-of-concept for solute entrapment and cargo release from the interior of these voluminous calcium-seamed nanocapsule assemblies, suggesting these synthetic hosts might act as controlled delivery vehicles for other guests such as (bio)pharmaceuticals, nutrients, preservatives, or antioxidants. These prospects are currently under exploration within our laboratories.

Conclusions

In summary, we have discovered a new family of nanocapsules self-assembled from pyrogallol[4]arene building blocks and calcium ions. These two structures show conserved geometry based on a Platonic solid (cube) but differ from all previous pyrogallol[4]arene nanocapsules in the number of PgC moieties, the role of the polyatomic metal ions in completely blocking the interior, and the high variability in the number, type, and connectivity of the seaming metal ions (and their counterions). These capsules possess a completely sealed and exceptionally large interior which our preliminary investigations suggest is stabilized against solvent loss more so than the interstitial space, further expanding the applicability of pyrogallol[4]arene capsules in the creation of discrete, fully-encapsulated nanoscale chambers. The complexity of the seaming polyatomic ions adds variability to the growing range of applications that nanocapsules have as high-nuclearity metal–organic clusters. We attribute the scarcity of examples of these capsules to the complexity of the polyatomic ions which play a critical role in capsule assembly but also the unpredictability in assembly, plus the fact that the structural characterization of supramolecules of this size is beyond the capabilities of many in-house single-crystal diffractometers. Nevertheless, we are confident that these examples represent the first of a diverse family of colossal nanocapsules, and we continue to search for the next examples.

Data availability

Crystallographic data in the ESI† have been deposited at the joint Cambridge Crystallographic Data Centre (CCDC **2**: 1955663; **3**: 2071418).

Author contributions

All authors approve the manuscript.

Conflicts of interest

There are no conflicts to declare.

Acknowledgements

We thank the Advanced Light Source, which is supported by the Director, Office of Science, Office of Basic Energy Sciences, of the U.S. Department of Energy. We also thank Dr David Stalla and the MU's Electron Microscopy Core "Excellence in Electron Microscopy Award" for assistance with SEM-EDS analysis.

Notes and references

1 R. Wyler, J. de Mendoza and J. Rebek Jr, *Angew. Chem., Int. Ed.*, 1993, **32**, 1699–1701.
2 N. Branda, R. Wyler and J. Rebek, *Science*, 1994, **263**, 1267–1268.
3 R. S. Meissner, J. Rebek and J. de Mendoza, *Science*, 1995, **270**, 1485–1488.
4 L. R. MacGillivray and J. L. Atwood, *Nature*, 1997, **389**, 469–472.
5 L. R. MacGillivray and J. L. Atwood, *Angew. Chem., Int. Ed.*, 1999, **38**, 1019–1034.
6 T. Gerkensmeier, *Eur. J. Org. Chem.*, 1999, **9**, 2257–2262.
7 J. L. Atwood, L. J. Barbour and L. A. Jerga, *Chem. Commun.*, 2001, **22**, 2376–2377.
8 G. W. V. Cave, J. Antesberger, L. J. Barbour, R. M. McKinlay and J. L. Atwood, *Angew. Chem., Int. Ed.*, 2004, **43**, 5263–5266.
9 R. M. McKinlay, G. W. V. Cave and J. L. Atwood, *Proc. Natl. Acad. Sci. U. S. A.*, 2005, **102**, 5944–5948.
10 A. S. Rathnayake, C. L. Barnes and J. L. Atwood, *Cryst. Growth Des.*, 2017, **17**, 4501–4503.
11 N. P. Power, S. J. Dalgarno and J. L. Atwood, *New J. Chem.*, 2007, **31**, 17–20.
12 S. J. Dalgarno, N. P. Power, J. E. Warren and J. L. Atwood, *Chem. Commun.*, 2008, **13**, 1539–1541.
13 H. Kumari, A. V. Mossine, S. R. Kline, C. L. Dennis, D. A. Fowler, S. J. Teat, C. L. Barnes, C. A. Deakyne and J. L. Atwood, *Angew. Chem., Int. Ed.*, 2012, **51**, 1452–1454.
14 H. Kumari, C. L. Dennis, A. V. Mossine, C. A. Deakyne and J. L. Atwood, *ACS Nano*, 2012, **6**, 272–275.
15 J. L. Atwood, E. K. Brechin, S. J. Dalgarno, R. Inglis, L. F. Jones, A. Mossine, M. J. Paterson, N. P. Power and S. J. Teat, *Chem. Commun.*, 2010, **46**, 3484–3486.
16 A. S. Rathnayake, K. A. Feaster, J. White, C. L. Barnes, S. J. Teat and J. L. Atwood, *Cryst. Growth Des.*, 2016, **16**(7), 3562–3564.
17 R. M. McKinlay, P. K. Thallapally and J. L. Atwood, *Chem. Commun.*, 2006, **28**, 2956–2958.
18 R. L. McKinlay, P. K. Thallapally, G. W. V. Cave and J. L. Atwood, *Angew. Chem., Int. Ed.*, 2005, **44**, 5733–5736.
19 D. V. Wagle, S. P. Kelley, G. A. Baker, K. Sikligar and J. L. Atwood, *Angew. Chem., Int. Ed.*, 2020, **59**, 8062–8065.
20 A. S. Rathnayake, H. W. L. Fraser, E. K. Brechin, S. J. Dalgarno, J. E. Baumeister, J. White, P. Rungthanaphatsophon, J. R. Walensky, S. P. Kelley, C. L. Barnes and J. L. Atwood, *J. Am. Chem. Soc.*, 2018, **140**(46), 15611–15615.
21 A. S. Rathnayake, H. W. L. Frazer, E. K. Brechin, S. J. Dalgarno, J. E. Baumeister, P. Rungthanaphatsophon,

J. R. Walensky, C. L. Barnes and J. L. Atwood, *J. Am. Chem. Soc.*, 2018, **140**(40), 13022–13027.
22 A. S. Rathnayake, H. W. L. Fraser, E. K. Brechin, S. J. Dalgarno, J. E. Baumeister, J. White, P. Rungthanaphatsophon, J. R. Walensky, C. L. Barnes, S. J. Teat and J. L. Atwood, *Nat. Commun.*, 2018, **9**, 2119–2125.
23 K. Su, M. Wu, D. Yuan and M. Hong, *Nat. Commun.*, 2018, **9**, 4941.
24 L. Mei, P. Ren, Q. Y. Wu, Y. B. Ke, J. S. Geng, K. Liu, X. Q. Xing, Z. W. Huang, K. Q. Hu, Y. I. Liu, L. Y. Yuan, G. Mo, Z. H. Wu, J. K. Gibson, Z. F. Chai and W. Q. Shi, *J. Am. Chem. Soc.*, 2020, **142**, 16538–16545.
25 M. Chwastek, P. Cmoch and A. Szumna, *J. Am. Chem. Soc.*, 2022, **144**, 5350–5358.
26 H. Kumari, S. R. Kline, D. A. Fowler, A. V. Mossine, C. A. Deakyne and J. L. Atwood, *Chem. Commun.*, 2014, **50**, 109–111.
27 C. Zhang, K. Sikligar, R. S. Patil, C. L. Barnes, G. A. Baker and J. A. Atwood, *Chem. Commun.*, 2018, **54**, 635–637.
28 C. Zhang, K. Sikligar, R. S. Patil, C. L. Barnes, S. J. Teat and J. L. Atwood, *Chem. Commun.*, 2017, **53**, 9613–9615.
29 V. López, G. R. Pérez, A. Arregui, E. Mateo-Marti, L. Bañares, J. N. Martin-Gago, J. M. Soler, J. Gómez-Herrero and F. Zamora, *ACS Nano*, 2009, **3**, 3352–3357.
30 Z. Zhang, Y. Chen, X. Xu, J. Zhang, G. Xiang, W. He and X. Wang, *Angew. Chem., Int. Ed.*, 2014, **53**, 429–433.
31 X. Hu, S. Feng, J. Du, L. Shao, J. Lang, C. Zhang, S. P. Kelley, J. Lin, S. J. Dalgarno, D. A. Atwood and J. L. Atwood, *Chem. Sci.*, 2020, **11**, 12547–12552.
32 X. Hu, J. Chai, C. Zhang, J. Lang, S. P. Kelley, S. Feng, B. Liu, D. A. Atwood and J. L. Atwood, *J. Am. Chem. Soc.*, 2019, **141**, 9151–9154.
33 C. Zhang, F. Wang, R. S. Patil, C. L. Barnes, T. Li and J. L. Atwood, *Chem.–Eur. J.*, 2018, **24**, 14335–14340.
34 C. Zhang, R. S. Patil, C. L. Barnes and J. L. Atwood, *Cryst. Growth Des.*, 2017, **17**, 4541–4543.
35 C. Zhang, R. S. Patil, C. Lui, C. L. Barnes and J. L. Atwood, *J. Am. Chem. Soc.*, 2017, **139**, 2920–2923.
36 L. Shao, B. Hua, X. Hu, D. Stalla, S. P. Kelley and J. L. Atwood, *J. Am. Chem. Soc.*, 2020, **142**(16), 7270–7275.
37 K. Sikligar, S. P. Kelley, L. Shao, G. A. Baker and J. L. Atwood, *Cryst. Growth Des.*, 2021, **21**(4), 1891–1897.
38 K. Su, M. Wu, D. Yuan and M. Hong, *Nat. Commun.*, 2018, **9**, 4941–4946.
39 C. Zhang, R. S. Patil, T. Li, C. L. Barnes and J. L. Atwood, *Chem. Commun.*, 2017, **53**, 4312–4315.
40 C. Zhang, R. S. Patil, T. Li, C. L. Barnes, S. J. Teat and J. L. Atwood, *Chem.–Eur. J.*, 2017, **23**, 8520–8524.
41 K. Su, K. Su, M. Wu, W. Wang, M. Zhou, D. Yuan and M. Hong, *Science*, 2018, **61**, 664–669.
42 C. Zhang, R. S. Patil, C. L. Barnes and J. L. Atwood, *Chem. Commun.*, 2017, **53**, 12144–12147.
43 K. Sikligar, S. P. Kelley, G. A. Baker and J. L. Atwood, *Cryst. Growth Des.*, 2022, **22**(5), 2806–2811.
44 S. Xian, Y. Lin, H. Wang and J. Li, *Small*, 2021, **17**, 2005165.
45 G. G. Facas, V. Maliekkal, C. Zhu, M. Neurock and P. J. Dauenhauer, *JACS Au*, 2021, **1**(3), 272–281.
46 B. Röche, T. X. Gentner, J. Langer, C. Färber, J. Eyselein, L. Zhao, C. Ding, G. Frenking and S. Harder, *Science*, 2021, **371**(6534), 1125–1128.
47 P. Sobota, A. Drąg-Jarząbek, L. John, J. Utko, J. B. Jerzykiewicz and M. Duczmal, *Inorg. Chem.*, 2009, **48**(14), 6584–6593.
48 M. Almáši, V. Zeleňak, R. Gyepes, L. Zauška and S. Bourrelly, *RSC Adv.*, 2020, **10**(54), 32323–32334.
49 G. B. Deacon, P. C. Junk and J. Moxey, *Dalton Trans.*, 2010, **39**(16), 5620–5622.